Powder Technology 253 (2014) 178–186

Contents lists available at ScienceDirect

Powder Technology

journal homepage: www.elsevier.com/locate/powtec

Synthesis, characterization of mesoporous silica powders and application to antibiotic remotion from aqueous solution. Effect of supported Fe-oxide on the SiO_2 adsorption properties

Maximiliano Brigante [a,*], María E. Parolo [b], Pablo C. Schulz [a], Marcelo Avena [a]

[a] INQUISUR, Departamento de Química, Universidad Nacional del Sur, Av. Alem 1253, 8000 Bahía Blanca, Argentina
[b] Facultad de Ingeniería, Universidad Nacional del Comahue, Neuquén 8300, Argentina

ARTICLE INFO

Article history:
Received 24 July 2013
Received in revised form 19 September 2013
Accepted 6 November 2013
Available online 16 November 2013

Keywords:
Mesoporous silica
Iron oxide
Composed materials
Solid-water interface
Minocycline adsorption
Surface complexes

ABSTRACT

The remotion of the antibiotic minocycline (MC) on mesoporous silica (SiO_2) and on the binary system iron(III) oxide–SiO_2 (Fe-SiO_2) has been studied in batch experiments by performing adsorption isotherms/kinetics under different conditions of pH, KCl concentration and temperature. The adsorption of MC on the studied materials is strongly dependent on pH, increasing as pH decreases. The incorporation of a low concentration of iron (1.03 wt.%, mainly as amorphous Fe_2O_3) on the SiO_2 matrix not only increases the adsorption capacity but also changes the adsorption mechanism. The adsorption of MC on SiO_2 strongly decreases as KCl concentration increases but it is not significantly affected by varying the temperature. This is attributed to electrostatic attractions and H-bond formations between dimethylamino, amide, carbonylic and phenolic groups of the antibiotic and the functional groups of silica particles. The adsorption of MC on Fe-SiO_2, on the contrary, strongly increases as temperature increases but remains invariable by varying the KCl concentration. This suggests that the formation of inner-sphere complexes between the functional groups of the antibiotic and the active sites of Fe_2O_3 plays a key role on the adsorption mechanism. The analysis of adsorption thermodynamic parameters is also reported and discussed. The synthesized materials can act as excellent adsorbents for environmental and engineering processes.

1. Introduction

Minocycline (MC) is a semi-synthetic tetracycline antibiotic that is able to pass the blood–brain barrier and is safe for clinical use. In addition to its antibacterial activity, MC also has anti-inflammatory, anti-oxidative, anti-apoptotic and neuroprotective properties [1]. It is known that only a small portion of this antibiotic can be metabolized or absorbed in vivo, while the rest of it is released in excreta [2]. Therefore, as a consequence of the application of livestock wastes to agricultural fields, antibiotics such as MC may be accumulated in soils or transported to groundwater. Although the maximum permissible concentration of MC (and other tetracyclines) in aqueous solutions for industrial and pharmacy wastewaters is very low (1 μgL^{-1}), Pena et al. [3] reported that concentrations of 15 μgL^{-1} MC could be detected in wastewater effluents. Moreover, there is a growing environmental concern about antibiotics because their presence in soils and waters leads to the emergence of resistant species [4]. Accordingly, it is very important to understand the fate of MC and other tetracycline contaminants in the water–soil environment in order to better assess their risks and develop mitigation strategies [5].

The interactions between bioactive molecules and synthetic adsorbents constitute an area of research of extreme importance in the field of straightforward technological applications as well as in basic science [6]. In this respect, mesoporous silica can be a good adsorbent due to its high surface area (>200 m^2g^{-1}), ordered frameworks, narrow pore size distribution (2 – >10 nm, higher than zeolites), and high thermal stability [7–9]. Due to these properties, mesoporous silicas are widely used in catalysis, separation, drug delivery, chemical sensing, optic and electronic applications, reinforcing of rubber, and as template in the synthesis of nanomaterials [10,11]. It is well known that the pore morphology of silica and its reactivity towards different molecules strongly depends on the synthesis conditions, e.g., pH, temperature, type and concentration of surfactant used as template, etc. [12]. Turku et al. [13], for example, show a strong and irreversible adsorption of tetracycline on comercialllly mesoporous SiO_2 (Merck, surface area = 700 m^2g^{-1}) whereas the adsorption of the antibiotic on another mesoporous SiO_2, synthesized in our laboratory in alkaline media using cetyltrimethylammonium bromide (CTAB) surfactant as template (surface area = 238.6 m^2g^{-1}), was almost negligible [14].

Surface-functionalized mesoporous silicas with metals and/or metal oxides have recently been studied in order to improve the SiO_2 adsorption capacity. In this sense, mesoporous silica modified with titania

* Corresponding author. Tel.: +54 291 4595101x3593.
E-mail address: brigante@uns.edu.ar (M. Brigante).

0032-5910/$ – see front matter © 2013 Elsevier B.V. All rights reserved.
http://dx.doi.org/10.1016/j.powtec.2013.11.008

nanoparticles shows a very strong adsorption capacity towards antibiotics and pesticides in comparison with the bare SiO_2 [14,15]. The adsorption was attributed to a direct binding of these adsorbates to TiO_2 leading to the formation of surface species of the type SiO_2–TiO_2 adsorbate. From these studies the authors also revealed that the adsorption capacity increases in the order $TiO_2 < TiO_2$–SiO_2 mainly due to the highly surface area that the silica offers and to the homogenously dispersion of the TiO_2 crystallites over the surface, or inside the mesopores, which prevents or reduces the aggregation of them [14].

Iron(III) species are also widely used as active components for removing pollutants from water [16,17]. In fact, ferrihydrite, goethite and amorphous ferric oxide as individual components are frequently used due to its low cost and high reactivity. However, most of them incorporate sedimentation which creates difficulty in solid/liquid separation [18]. Thus, the synthesis of iron(III) oxide-silica materials, as produced in the present work, can result suitable to overcome these difficulties. Moreover, several reports showed that iron(III) oxide supported in mesoporous silica strongly enhances the adsorption of phosphorous and arsenic from drinking water [16,18]. The mechanism is mainly related to the formation of inner-sphere complexes between the adsorbate (mostly in the form of arsenate or phosphate) and Fe^{3+} hydrated species. Silicas modified with iron(III) oxide are also known to be used as humidity sensors [19], as platforms in the synthesis of carbon nanotubes [20], and as catalysts [21] with very good results.

The aim of this article is to present a comparative study of adsorption of the antibiotic minocycline on mesoporous SiO_2 and on the binary system iron(III) oxide–SiO_2 (Fe-SiO_2) in order to evaluate the effect of iron species on the morphology and adsorption properties of silica. The adsorption data obtained at different pH, KCl concentrations, and temperatures are used to gain insights into the mechanisms that govern the adsorption process and into the factors that promote or prevent adsorption.

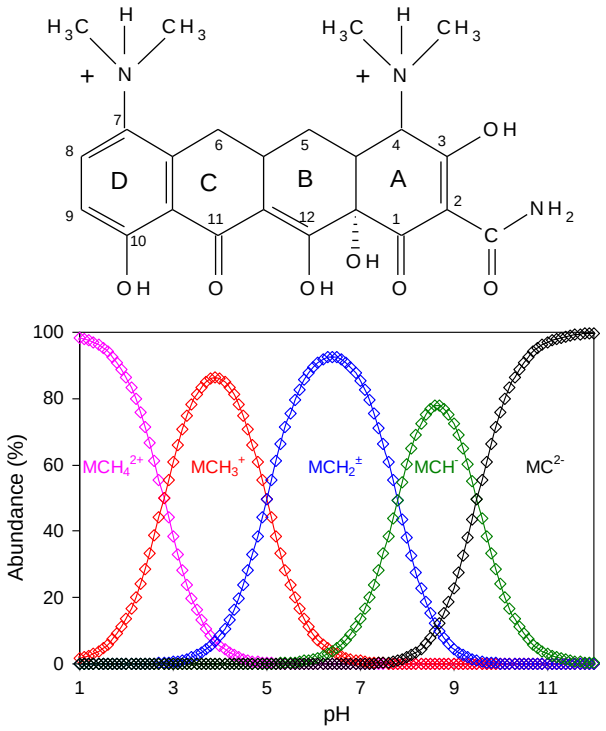

Fig. 1. Molecular structure of fully protonated minocycline and its speciation under different pH values in aqueous solution.

2. Materials and methods

2.1. Chemicals

Cetyltrimethylammonium *p*-toluene sulfonate or tosylate (CTAT, MW = 455.7 $gmol^{-1}$), Pluronic F68 and tetraethyl orthosilicate (TEOS, 99%) were purchased from Aldrich. Iron(III) nitrate nonahydrate, potassium hydroxide, potassium chloride, potassium nitrate, nitric acid, hydrochloric acid, sodium acetate, acetic acid, sodium carbonate, sodium hydrogen carbonate, disodium phosphate anhydrous, and monosodium phosphate anhydrous were obtained from Anedra.

Minocycline hydrochloride was purchased from PARAFARM. The structural formula of MC is shown in Fig. 1. In aqueous solutions five different groups of the molecule can undergo protonation–deprotonation reactions depending on the pH of the solution giving rise to the formation of four different species. The fully protonated species of MC exists at low pH values (MCH_4^{2+}). As the pH increases, the first deprotonation step (pKa = 2.8) occurs at the hydroxyl group on C3 leading to the formation of a species with a positive charge (MCH_3^{+}). The second deprotonation step (pKa = 5.0) takes place in the aromatic amino group generating a zwitterionic species ($MCH_2^{\pm}$). The third deprotonation (pKa = 7.8) involves the O10–O12 ketophenolic hydroxyl group giving rise to a species with a negative charge (MCH^{-}). Finally, the fourth deprotonation (pKa = 9.5) involves the dimethylamino group giving rise to a species with two negative charges (MC^{2-}) [22].

All chemicals were of analytical grade and used as received. Doubly distilled water was used for the preparation of solutions.

2.2. Synthesis and characterization of SiO_2 and Fe-SiO_2

Mesoporous silica was prepared using a procedure similar to that described in an earlier work [12]. Briefly, 11.6 mL of TEOS were mixed with 2 mL of water and stirred in an autoclave flask for 10 min at 500 rpm. At the same time, 38 mL of CTAT-Pluronic F68 mixed solution were prepared with a 0.75:0.25 M ratio by adding the desired amount of surfactants to water. This mixture was stirred in a conical flask at 35 °C to form a transparent template solution and then it was left at room temperature. To obtain the mesoporous material, 20 mL of a 1.43 M HCl solution were added drop by drop to the TEOS solution under stirring and 2 min later the surfactant solution was incorporated. The resulting gel, whose composition was 1 TEOS:0.53 HCl:0.011 CTAT:0.0037 F68, was stirred for 5 min and then left for 48 h in an autoclave at 100 °C. After this, the gel was filtered and washed with distilled water and dried at room temperature. Finally, it was calcined in an air flux by increasing the temperature from room temperature to 540 °C with a heating rate of 2°Cmin^{-1}, and holding for 7 h at 540 °C.

Fe-SiO_2 was synthesized by a simple batch equilibrium adsorption method. In a beaker, 2 g of calcined SiO_2 were mixed with 40 mL of a 0.13 M $Fe(NO_3)_3$ solution and stirred for 1 h at 600 rpm. Then, the solid was filtered and washed with water and dried at room temperature. Finally, it was calcined in an air flux for 2 h at 540 °C. The iron content on the silica support was 10.3 mgg^{-1} (1.03 wt.%), which was measured by UV–VIS spectroscopy using the thiocyanate colorimetric method [23] after extracting the Fe(III) ions from the solid with concentrated HNO_3 [24].

The synthesized materials were characterized by the techniques usually employed in porous materials, such as scanning and transmission electron microscopy (SEM and TEM); XRD; FT-IR spectroscopy; electrophoretic mobility measurements; and the N_2-BET method for surface area, pore volume and pore diameter determination. SEM was performed using an EVO 40-XVP microscope. The samples were prepared on graphite stubs and coated with a ca. 300 Å gold layer in a PELCO 91000 sputter coater. TEM was performed using a JEOL 100 CX II transmission electron microscope, operated at 100 kV with magnification of 450000×. Observations were made in a bright field. The powdered samples were placed on 2000 mesh copper supports. XRD patterns were obtained via a Philips PW 1710 diffractometer with

CuKα radiation (λ = 1.5406 Å) and graphite monochromator operated at 45 kV, 30 mA and 25 °C. The electrophoretic mobilities of SiO_2 and Fe-SiO_2 were measured with a Zetasizer Nano Series instrument (Malvern Instruments Ltd.) at room temperature, and the Zeta potentials were calculated using the Smoluchowski equation. Stock suspensions containing 0.1 gL^{-1} of solid in 10^{-2} M KNO_3 were used for the measurements. The pH of the suspensions was adjusted to the desire value by adding small volumes of HNO_3 or KOH solutions. The N_2 adsorption isotherms at 77.6 K were measured with a Quantachrome Nova 1200e instrument. The samples were degassed at 373 K for 720 min at a pressure of 1×10^{-4} Pa. FT-IR experiments were recorded in a Nicolet FT-IR Nexus 470 Spectrophotometer. To avoid co-adsorbed water the samples were dried under vacuum until constant weight and then they were diluted with KBr powder before the FT-IR spectrum was recorded.

2.3. Adsorption experiments

Adsorption experiments (in darkness to avoid photodegradation) were obtained with a batch equilibration procedure using 15 mL polypropylene centrifuge tubes covered with polypropylene caps immersed in a thermostatic shaker bath. Before starting the experiment, a stock MC solution (2×10^{-3} M) was prepared by adding the corresponding solid to buffer solutions. The pHs investigated were 4.4 (0.1 M acetate/acetic acid), 7.0 (0.1 M $HPO_4^{2-}/H_2PO_4^-$), and 9.5 (0.1 M CO_3^{2-}/HCO_3^-). 50 mg of mesoporous material were introduced into the tubes and mixed with varying quantities of MC and KCl (used as supporting electrolyte) solutions. The range of initial MC concentration was 5×10^{-5}–2×10^{-3} M, and the final volume was 10 mL. The stirring rate was kept constant at 90 rpm. At different reaction times, the particles were separated from the supernatant by centrifugation at 4000 rpm during 2 min and the supernatant was immediately analyzed to quantify the concentration of adsorbed MC. After the quantification (see below), which took around 30 s, the supernatant was reintroduced into the tube. This procedure (separation, quantification of MC and reintroduction of the supernatant into the reaction tube) was repeated during several hours in order to achieve complete adsorption of the antibiotic or to gather enough data points. The last data point obtained in these experiments was assumed to represent equilibrium conditions. Adsorbed MC was calculated from the difference between the initial MC concentration and the concentration of the antibiotic that remained in the supernatant solution. In most experiments no supporting electrolyte was used and the working temperature was 25 °C (except when effects of KCl concentration and temperature were investigated).

To evaluate the effect of phosphate buffer on the adsorption of MC, the experiments were carried out in water and at pH 7 by adding HCl or KOH solutions. Before starting the experiment, a stock MC solution (2×10^{-3} M) was prepared by adding the corresponding solid to double distilled water. Its pH was then adjusted to the desired value by adding HCl or KOH solutions. Then, 50 mg of mesoporous material were introduced into the tubes and mixed with varying quantities of the MC solution and water (previously adjusted at pH 7). During the time when the suspensions were mixed, the pH was checked and kept constant by adding small volumes (microliters) of concentrated KOH or HCl solutions.

Quantification of MC was performed by UV–VIS spectroscopy at 354 nm for pH 4.4, at 345 nm for pH 7, and at 382 nm for pH 9.5 using an Agilent 8453 UV–VIS diode array spectrophotometer equipped with a Hellma 1 cm quartz cell. This is due to the shifting of the maximum absorption band of MC as pH varies [25]. The supernatant of the withdrawn aliquot was placed into the cell and the spectrum was recorded in the 200–900 nm wavelength range. Calibration curves at the working pH were conducted with several MC solutions having concentrations that ranged between 5×10^{-6} and 2×10^{-3} M. Very good linearity was found in all cases ($r^2 > 0.998$).

The adsorption kinetic is traditionally described following the expressions of the pseudo-first and the pseudo-second order equations originally given by Lagergren, which are special cases for the general Langmuir rate equation [26]. The pseudo-second order model, described by Eq. (1), was used here and in most solid/solution interaction studies [27]:

$$\frac{t}{q_t} = \frac{1}{k_{2,s} q_e^2} + \frac{1}{q_e} t. \quad (1)$$

where $k_{2,s}$ is the pseudo-second-order rate constant (gμmol^{-1} min^{-1}); and q_e and q_t (μmolg^{-1}) denote the amount of antibiotic adsorbed at equilibrium and at the reaction time t, respectively. The fitting validity of this model is traditionally checked by the linear plots of t/q_t versus t. The slope and intercept of the obtained straight line provide the respective kinetic constant and the q_e parameter.

Despite the Lagergren kinetic equations have been used in a great deal of adsorption kinetic works, this model cannot give interaction mechanisms, so another model was also used to test antibiotic adsorption on the studied materials. An intraparticle diffusion model (Morris–Weber model), described by Eq. (2), was examined [27]:

$$q_t = k_{int} t^{0.5} + I, \quad (2)$$

where k_{int} is the intraparticle diffusion rate constant and I is the intercept. I is also an indicator about the thickness of boundary layer, i.e., the larger the intercept, the greater the boundary layer effect. According to the model, if intraparticle diffusion is the rate-limiting step of the whole adsorption process, the plot of q_t versus $t^{0.5}$ yields a straight line passing through the origin. Otherwise, some other mechanisms are possibly involved along with intraparticle diffusion.

The adsorption isotherms were fitted using both Langmuir and Freundlich equations, which were commonly used in the adsorption of antibiotics on several adsorbent systems [28,29]. The linear forms of these equations are displayed as Eqs. (3) Langmuir and (4) Freundlich:

$$\frac{1}{MC_{ads}} = \frac{1}{q_{mon}} + \frac{1}{q_{mon} K_L MC_{eq}} \quad (3)$$

$$\ln MC_{ads} = \ln K_F + \frac{1}{n} \ln MC_{eq}, \quad (4)$$

where MC_{ads} is the adsorbed amount of MC (μmolg^{-1}); MC_{eq} is the equilibrium concentration of MC in the supernatant (μM); q_{mon} is the maximum amount of antibiotic adsorbed (μmolg^{-1}) corresponding to complete coverage on the surface; K_L and K_F are the Langmuir and Freundlich constants (μM^{-1}), respectively; and $1/n$ is the adsorption intensity. From the linearized form of Eqs. (3) and (4), q_{mon}, K_L, K_F, $1/n$, and the correlation coefficient, r^2, can be calculated.

3. Results and discussion

3.1. General characteristics of the synthesized materials

The synthesized mesoporous SiO_2 particles had a characteristic white colouration, while Fe-SiO_2 was a yellowish/light brown powder, as shown in the Supplementary Material (SM, see SM Fig. S1), confirming the presence of iron oxide in the adsorbent matrix.

Fig. 2 shows the electronic micrographs of the synthesized samples. According to the SEM images, SiO_2 consists of agglomerates of polydisperse spheres (Fig. 2a). The morphology of Fe-SiO_2 (Fig. 2c) is similar to that of the silica support and there is no evidence of separate iron(III) oxide crystallites. This may indicate the formation of fine particles (mainly as Fe_2O_3) and their dispersion over the SiO_2 surface or into the mesopores. The formation of Fe_2O_3 on mesoporous silica was demonstrated in several works [19,30], where a triblock copolymer was

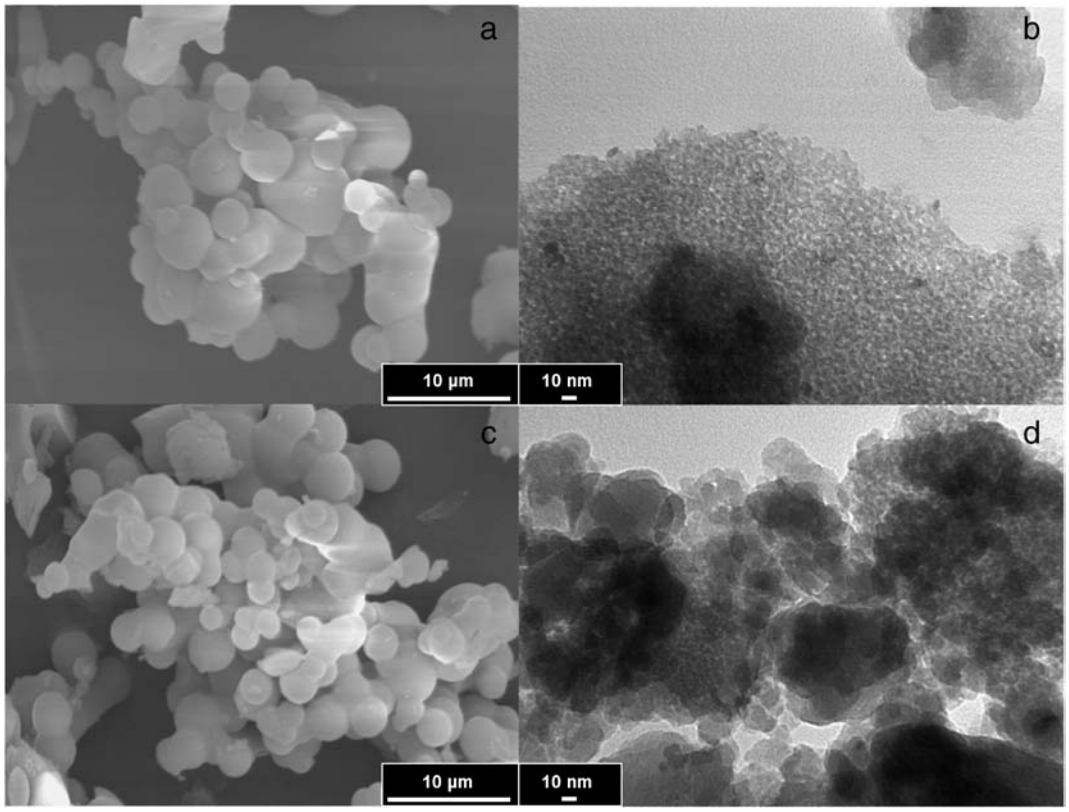

Fig. 2. SEM (20000×, left side) and TEM (450000×, right side) micrographs of: (a and b) SiO_2, and (c and d) Fe-SiO_2.

used as template, TEOS and $Fe(NO_3)_3$ were used as silica and iron oxide precursors, respectively, and where the resulting solid was calcined in air-flux furnace at 550 °C. The porous structure of the synthesized materials is evidenced by TEM images. Fig. 2b and d show that SiO_2 and Fe-SiO_2 contain mesopores, with pore diameters of around 3.10 nm.

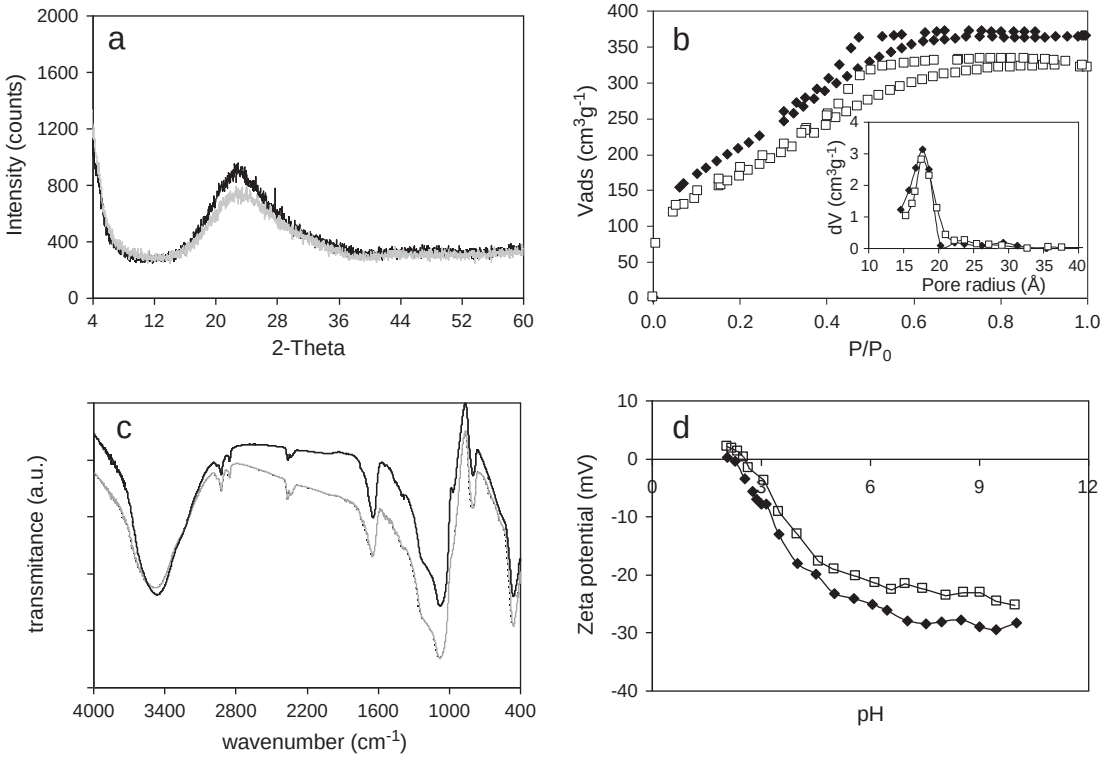

Fig. 3. Characterization of studied sample by: (a) XRD; (b) N_2 adsorption–desorption isotherms, where the inset shows the pore radius distribution; (c) infrared spectroscopy; and (d) electrophoretic mobility measurements as a function of pH in a 10^{-3} M KNO_3 solution. Black line and solid diamonds, SiO_2; and gray line and open squares, Fe-SiO_2.

The results obtained by XRD, nitrogen sorption isotherms, FT-IR spectroscopy and electrophoretic mobility are shown in Fig. 3a–d, respectively. SiO_2 shows a XRD pattern typical of amorphous materials, which is also characteristic of mesoporous silicas [14]. The mesoporous structure of SiO_2 is stable under our synthesis conditions and it does not collapse during calcination at 540 °C resulting in the transformation to the cristobalite phase, as observed by Gu et al. [31]. Fe-SiO_2 shows a very similar XRD pattern, and no peaks of crystalline iron(III) oxides are observed. The question that arises about the Fe_2O_3 phase is whether it is present as a true amorphous phase or as small and undetectable nanocrystalline particles. It is known that nanoparticles of amorphous Fe_2O_3 crystallize into nanocrystalline maghemite (γ-Fe_2O_3) at around 300 °C, whereas the same transformation occurs at higher temperatures (700 °C or higher) for Fe_2O_3–SiO_2 amorphous nanoparticles [32]. The observed shift is related to the stabilization of the amorphous Fe_2O_3 nanophase due to preventive role of the silica matrix [30]. However, since our sample was calcined at 540 °C and there were not evidence of crystallite Fe-oxide phase from the XRD studies, only the presence of amorphous Fe-oxide can be suggested. Similar results were reported by Ennas et al. [33] and Gervasini et al. [34] for Fe_2O_3–SiO_2 materials at several Fe loadings.

The nitrogen sorption isotherms of SiO_2 and Fe–SiO_2 are typical type IV isotherms with H2 hysteresis loop, corresponding to a non-defined distribution of pore sizes and shapes, which appear in several inorganic oxide gels, glasses, and mesoporous silica as SBA − 16 [35,36]. This was attributed in the past to “ink bottle pores”, but it is now recognized that this description provides an oversimplified picture of the actual situation, and that the role of network effects must be taken into account [37]. The calculated BET surface area and pore volume were 773 m^2g^{-1} and 0.564 cm^3g^{-1} for SiO_2, and 632 m^2g^{-1} and 0.510 cm^3g^{-1} for Fe-SiO_2, respectively. The observed decrease in these parameters is attributed to the coverage of the silica surface by the Fe-oxide phase, leading to a material with reduced surface area and smaller porosity than SiO_2 [32]. The well-defined step that occurs at P/P_0 between 0.5 and 0.6, corresponding to capillary condensation of N_2, indicates the uniformity of the pores, as shown in the inset of Fig. 3b. In fact, the pore radii were sharply distributed in a narrow range located at approximately 1.77 nm and 1.62 nm for SiO_2 and Fe-SiO_2, respectively. This uniformity on the pore size is mainly attributed to the use of the F68 triblock copolymer in the material synthesis [12].

The most important features of the FT-IR spectra of SiO_2 are: a broad band centered at 3465 cm^{-1} associated to OH stretching of surface hydroxyls bound to silicon (Si – OH); a peak at 1646 cm^{-1} due to the OH bending mode of water molecules; a broad peak located at 1078 cm^{-1} with a shoulder at 1195 cm^{-1} which are attributed to asymmetric Si – O – Si vibrations; a peak centered at 798 cm^{-1} due to symmetric Si – O – Si vibrations; and peaks at 968 and 459 cm^{-1} assigned for Si–O–Si bending modes [38]. Characteristic bands at around 595 and/or 960 cm^{-1}, attributed to Fe – O – Fe bending and Si – O – Fe stretching modes, respectively, were not detected on the FT-IR spectrum of Fe-SiO_2. Liu et al. [39] reported that these bands can only be detected in Fe-SiO_2 samples with 9 wt.% Fe or higher. However, these authors showed a slightly modification of the 968 cm^{-1} SiO_2 peak which is attributed to the presence of Si – O – Fe species in agreement with our results, i.e., a shift of this band towards higher wavenumbers.

The Zeta potential vs. pH data show that the mesoporous SiO_2 has an isoelectric point (IEP) of 2.1, whereas the IEP of Fe-SiO_2 is slightly higher (2.8). The IEP of silica is in agreement with those reported in the literature ([40], and references therein). It is known that the IEP of Fe_2O_3 is between pH 7.5 − 8.5 ([40], and references therein). Therefore, the small shift of IEP from 2.1 to 2.8 indicates that only a small fraction of the silica surface was covered with iron oxides, and that most of the charging behavior is dominated by the SiO_2 surface. Similar results were reported by Rufier et al. [41] and Xu and Axe [42] on the synthesis of hematite- and goethite-coated silicas, respectively.

3.2. MC adsorption studies

Adsorption kinetics of MC on SiO_2 and Fe-SiO_2 as a function of pH are shown in Fig. 4. The adsorption is very fast between t = 0 and t = 5 min in almost all experiments (Fig. 4a). It is so fast that no data point could be measured in this period with our experimental set up. At t > 5 min the adsorption takes place at a much slower and measurable rate, and at around 250 min equilibrium seems to be reached in all cases. The adsorption capacity increases in the order SiO_2 < Fe-SiO_2 suggesting that Fe_2O_3 nanoparticles dispersed on the silica surface or inside the mesopores offer more active sites for adsorption than the silica support. Fig. 4a also shows that the adsorption on both adsorbents is strongly dependent on the pH. It is relatively high at low pH and decreases significantly. All data were well-fitted by the pseudo-second order model (Eq. 1) with $r^2 > 0.99$, as shown in Table 1. The q_e and $k_{2,s}$ values are much higher than those reported in a previous paper on the adsorption of a tetracycline antibiotic on mesoporous SiO_2 and on the binary system TiO_2–SiO_2 at the same experimental conditions, where the silica support was synthesized in alkaline media by using the cationic surfactant CTAB as template [14], revealing that the synthesis conditions and the type of metal and/or metal oxide supported play an important role on the reactivity of mesoporous silica. Therefore, the obtained results show that both SiO_2 and Fe-SiO_2 act as very good adsorbents for MC kinetically (and probably for other tetracyclines).

If the Weber–Morris model is applied to our results, as shown in Fig. 4b, at least three linear sections with different slopes are obtained. The multilinearity indicates that three steps occur in the sorption process. The first is commonly attributed to the boundary layer diffusion. The second is attributed to the gradual or slow adsorption stage where intra-particle diffusion is the rate limiting step; this step was

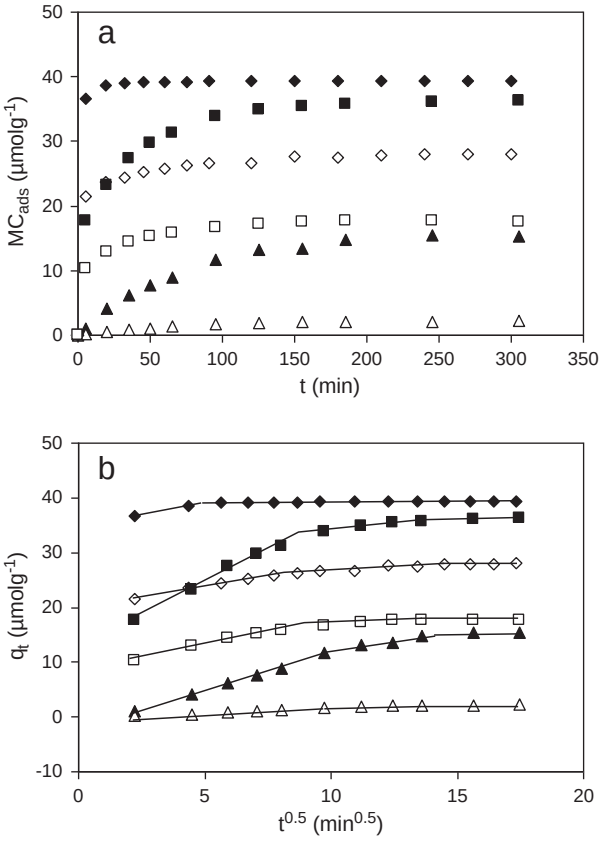

Fig. 4. Effect of pH on the adsorption kinetics of MC on SiO_2 (open symbols) and Fe-SiO_2 (solid symbols) at 25 °C: (a) adsorption rate, and (b) q_t versus $t^{0.5}$ for intraparticle diffusion model. pH values: diamonds, pH 4.4; squares, pH 7.0; and triangles, pH 9.5.

Table 1
Kinetic adsorption parameters for MC adsorption on the studied materials.

Pseudo-second-order model						
	SiO_2			Fe-SiO_2		
pH	q_e (μmolg^{-1})	$k_{2,s} \times 10^3$ (gμmol^{-1}min^{-1})	r^2	q_e (μmolg^{-1})	$k_{2,s} \times 10^3$ (gμmol^{-1}min^{-1})	r^2
4.4	28.41	6.84	1.00	39.37	119.47	1.00
7.0	18.25	6.37	1.00	37.59	2.44	1.00
9.5	2.92	4.38	0.99	19.72	0.70	0.99

Intraparticle difussion model						
	SiO_2			Fe-SiO_2		
pH	k_{int1}	k_{int2}	k_{int3}	k_{int1}	k_{int2}	k_{int3}
4.4	0.87 (0.98)	0.33 (0.95)	0.04 (1.00)	0.72 (0.96)	0.02 (0.94)	0.00 (0.14)
7.0	1.15 (1.00)	0.47 (0.99)	0.07 (1.00)	2.39 (0.99)	0.60 (0.98)	0.13 (0.98)
9.5	0.18 (1.00)	0.20 (0.98)	0.03 (0.82)	1.41 (1.00)	1.37 (0.99)	0.15 (1.00)

Note. In parentheses the respectively r^2 values are shown.

also ascribed to the diffusion of pharmaceuticals in mesopores [43]. The third is related to the final equilibrium stage where intra-particle diffusion further slows down due to the extremely low concentrations of adsorbate left in the solutions [43]. The results suggest, therefore, that the mechanism of MC adsorption over the surface of the studied solids is complex and both the surface adsorption as well as intraparticle diffusion contribute to the actual adsorption process. Table 1 also shows the k_{int} values which are obtained from the slopes of Fig. 4b.

The effect of pH on the adsorption can be better observed in the respective adsorption isotherms, as shown in Fig. 5. As expected, the adsorption is relatively high at pH 4.4 and decreases significantly at pH 7 and 9.5 indicating that the affinity of MC for both SiO_2 and Fe-SiO_2 is higher at low pH. Since at a given pH the adsorption of MC on Fe-SiO_2 is higher than on SiO_2, the increase in adsorption can be attributed to the direct binding of the antibiotic to the supported Fe_2O_3.

According to Fig. 1, the main species of MC in aqueous solution at pH 4.4, 7 and 9.5 are MCH_3^+, $MCH_2^{\pm}$, and MCH^- and MC^{2-}, respectively. SiO_2 and Fe- SiO_2 have negative surface charges at all studied pH. Thus, the adsorption of MC on SiO_2 at pH 4.4 is easy to be understood since interaction by electrostatic attraction should drive the MCH_3^+ species to the negatively charged SiO_2. As pH increases, these interactions decrease mainly due to a decrease in MCH_3^+ concentration and/or an increase in $MCH_2^{\pm}$, MCH^- or MC^{2-} concentration. The case of the last three species is somewhat different since the net charge of the molecules is respectively 0, −1, and −2. A simple electrostatic analysis considering only the net charge of these species indicates that $MCH_2^{\pm}$ should not be electrostatically attracted by SiO_2 and that MCH^- and MC^{2-} should be repelled by the surface. However, since $MCH_2^{\pm}$ and MCH^- species contain a positively charged group in their structure, it is likely that the molecules arrange at the surface so that the positively charged group is located very closed to the surface, leading the negatively charged one(s) as far as possible from the surface [22].

Fig. 5 also shows that at pH 7 the adsorption isotherm on Fe-SiO_2 is the same in the presence or absence of buffer, suggesting that phosphate ions do not compete with MC for the adsorption sites. It is known that phosphate ions compete with different adsorbates (carbonate, arsenate, pesticides such as glyphosate, etc.) for the adsorption active sites of several adsorbents and specially iron oxides and oxyhydroxides (e.g. goethite, ferrihydrite, etc.) [16,44,45]. However, all mentioned Fe-oxides have an IEP at around pH 7–9.5 and, therefore, the interaction phosphate-adsorbent (e.g., by formation of inner/outer-sphere complexes, ligand exchange, etc.) is expected to be more strongly than in SiO_2 (negligible or not exist) or in Fe-SiO_2, where both solids have an IEP lower than pH 2.5, i.e., the solids are negative-surface charged at pH 7. Besides, the low content of Fe-oxide in Fe-SiO_2 (1.03 wt.%) suggests that the effect of phosphate ions on MC adsorption is very low or no detectable by UV–VIS spectroscopy. Similar effects are expected by using acetate and carbonate buffers and thus the experiments at pH 4.4 and 9 without buffer were not performed. In fact, it was reported in literature that carbonate and acetate ions have a weak effect on the adsorption of tetracycline on a Fe-polyvinylpyrrolidone and on a Fe–Mn binary oxide [46,47]. Moreover, carbonate is known to be a weak competitor for the adsorption of anionic species (e.g., phosphate, arsenate, arsenite) on Fe-oxides [44,45].

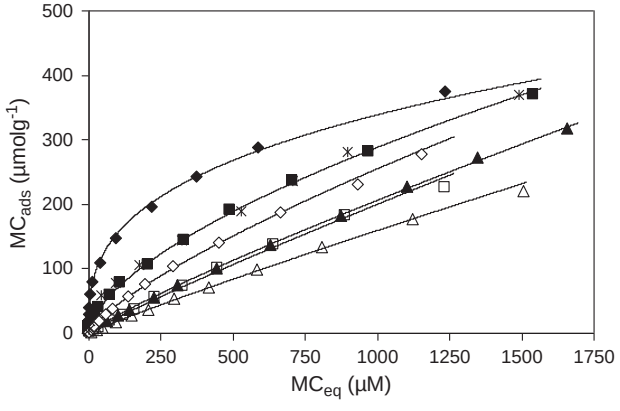

Fig. 5. Effect of pH on the adsorption of MC on SiO_2 (open symbols) and Fe-SiO_2 (solid symbols) at 25 °C. pH values: diamonds, pH 4.4; squares, pH 7.0; and triangles, pH 9.5. Slashes show the adsorption of MC on Fe-SiO_2 in absence of phosphate buffer. Lines show predictions of Eq. (3).

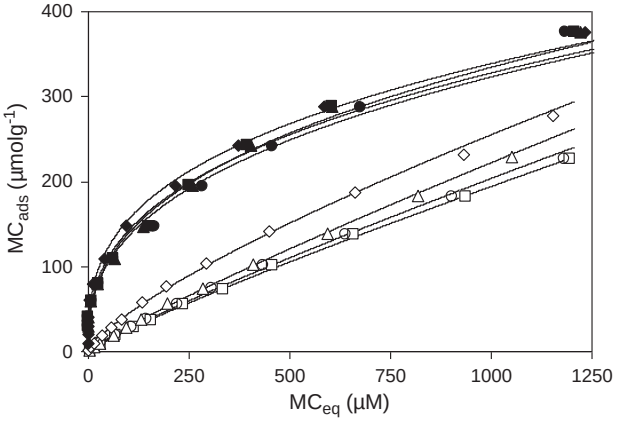

Fig. 6. Effect of KCl concentration on the adsorption of MC on SiO_2 (open symbols) and Fe-SiO_2 (solid symbols) at pH 4.4 and 25 °C. KCl concentrations: diamonds, 0 M; triangles, 0.01 M; circles, 0.1 M; and squares, 0.3 M. Lines show predictions of Eq. (3).

These results are supported by a decrease in the critical stability constants of both surface and aqueous complexes in the order Fe(III)-acetate < Fe(III)-carbonate < Fe(III)-phosphate [44,45,48].

Although the electrostatic interactions may play an important role in the adsorption of MC on both SiO_2 and Fe-SiO_2, there may also exist non-electrostatic interactions between the organic species and the solid surface [49]. These interactions, such as hydrogen bonding, surface complexation and van der Waals interaction are likely to operate not only with cationic species (MCH_3^+) but also with $MCH_2^{\pm}$, and MCH^- and MC^{2-} and they will contribute to the adsorption.

In order to analyze the hyphotesis mentioned above, Fig. 6 shows the effects of ionic strength (KCl concentration) on the adsorption of MC isotherms on SiO_2 and Fe-SiO_2 at pH 4.4 and 25 °C. The adsorption on SiO_2 depends on the precense of electrolyte, decreasing as KCl concentration increases. Even though the effect is not very strong, the results suggest that formation of outer-sphere complexes (or ionic pairs) is taking place on SiO_2, and competition between MC (as MCH_3^+, see Fig. 1) and K^+ for negatively charged groups occurs, leading to a decrease in MC adsorption by increasing K^+ concentration. Results resemble those reported in a previous work [25] for the adsorption of MC on ceria nanoparticles, where competition between the antibiotic and potassium ions was proposed to play a key role. On the other hand, the adsorption on Fe-SiO_2 does not depend on KCl concentration, suggesting a different adsorption process. It is known that the adsorption of several species on supported and unsupported Fe_2O_3 is related to the formation of inner-sphere complexes between the adsorbate and the active sites of the iron oxide [50,51] and, thus, they are expected to form in our system. In fact, Gu and Karthikeyan [52] reported that the antibiotic tetracycline forms inner-sphere complexes with both iron and aluminium hydrous oxides due to its tricarbonylamide (C1:C2:C3 in ring A) and carbonyl (C11 in ring C) functional groups.

The effects of temperature on the adsorption of MC on SiO_2 and Fe-SiO_2 at pH 4.4 are shown in Fig. 7. MC adsorption on SiO_2 is not significantly affected by varying the temperature from 15 to 45 °C. The weak dependence of the adsorption of MC with the temperature is consistent with formation of outer-sphere complexes or ionic pairs, where there is competition with the cations of the supporting electrolyte. If changes in temperature affect in a similar way the affinity of MC (as MCH_3^+ at pH 4.4) and K^+ for negatively charged sites, there will be no significant temperature effects. Similar results were reported in previous works for the adsorption of two cationic species on TiO_2–SiO_2 [14,15]. On the contrary, MC adsorption on Fe-SiO_2 increases as temperature increases reinforcing the fact that a chemisorption-like process may play an important role in the antibiotic-adsorbent system, i.e., formation of inner-sphere complexes between the functional groups of the antibiotic and the active sites of Fe_2O_3. Similar results were reported by Tanis et al. [53] on the adsorption of tetracycline on iron oxides-coated quartz.

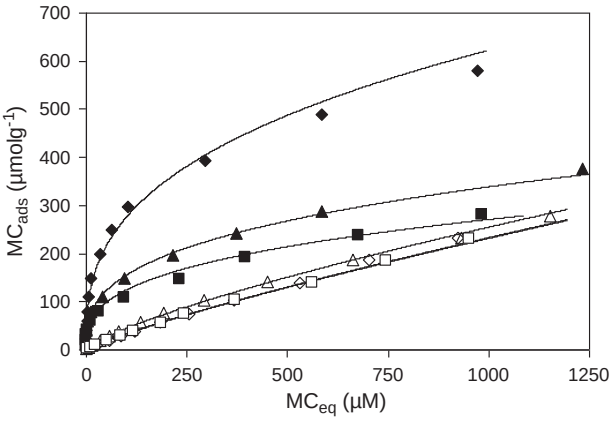

Fig. 7. Effect of temperature on the adsorption of MC on SiO_2 (open symbols) and Fe-SiO_2 (solid symbols) at pH 4.4 at pH 4.4. Temperatures: diamonds, 45 °C; triangles, 25 °C; and squares, 5 °C. Lines show predictions of Eq. (3).

Table 2
Thermodynamic parameters for MC adsorption on SiO_2.

T (°C)	$\Delta G°$(kJmol^{-1})	$\Delta H°$ (kJmol^{-1})	$\Delta S°$(JK^{-1} mol^{-1})
5	−15.44		
25	−16.59	0.52	57.44
45	−17.74		

From the data showed in Fig. 7 the thermodynamic parameters Gibbs free energy ($\Delta G°$), enthalpy ($\Delta H°$), and entropy ($\Delta S°$) for the adsorption of MC on the studied materials are obtained by using the following equations:

$$\Delta G° = -RT \ln K, \tag{5}$$

$$\ln K = \frac{\Delta S°}{R} - \frac{\Delta H°}{RT}, \tag{6}$$

where K is the equilibrium constant, T is the absolute temperature, and R is the gas constant (8.314 JK^{-1}mol^{-1}). The Langmuir isotherm can be applied to calculate the thermodynamic parameters assuming that $K = K_L$. $\Delta H°$ is obtained from van't Hoff plots as ln K_L versus 1/T. The thermodynamic parameters are shown in Table 2. Physisorption and chemisorption are sometimes classified by the magnitude of the enthalpy change. When $\Delta H°$ is in the range of (0–10) kJmol^{-1}, the adsorption mechanism is considered to be physisorption; i.e., the bond between adsorbent and adsorbate is due to van der Waals interactions. When $\Delta H°$ is in the range of (30–70) kJmol^{-1}, the adsorption is considered to be chemisorption; i.e., a chemical bond is formed between the adsorbate and the surface [54]. However, the above classification is commonly used to interpret adsorption at the solid–gas interface, which may significantly differ from the solid–liquid interface. In this last case, if a ligand exchange reaction takes place between the adsorbate and the functional groups of the surface the $\Delta H°$ values could be negative, positive or even zero (with magnitudes up to 70 kJmol^{-1}) and still be a chemisorption reaction [55,56]. The $\Delta H°$ value for the adsorption of MC on SiO_2 is positive implying that the interaction of MC with the solid is an endothermic process. The positive sorption entropy indicates an increased randomness at the solid–water interface during MC adsorption [53]. Finally, the negative value of $\Delta G°$ at various temperatures shows that the nature of adsorption on SiO_2 is spontaneous under standard conditions. Unfortunately, the thermodynamic parameters for the Fe-SiO_2 were difficult to predict, due to the bad fit achieved with the Langmuir equation ($r^2 < 0.8$ in all experiments, data not shown), and thus they are not reported. The bad fit can be attributed to the heterogeneity on the surface, where the Langmuirian parameters have limited applications [57].

Table 3 shows the best-fit parameters using Eqs. (3) and (4). The adsorption isotherms of MC on SiO_2 at pH 4.4 were well-fitted using both the Freundlich and the Langmuir adsorption isotherms. The last result is expected mainly because the Langmuir's theory assumes monolayer coverage of adsorbate over a homogenous adsorbent surface [14]. The maximum adsorption capacity on SiO_2 is 500 μmolg^{-1}, which is favorably compared with those using natural (or synthetic) adsorbents for removal tetracycline-type antibiotics, such as illite, rectorite, kaolinite, chitosan, goethite and Ca–montmorillonite [6,58,59]. On the contrary, the adsorption data points in the MC–Fe-SiO_2 system were better-fitted using the Freundlich equation which is related to adsorbents with a heterogeneous energy distribution of active sites. The Freundlich parameters also show that the adsorption conditions in all cases are favorable ($n > 1$).

Table 3
Values of the Langmuir and Freundlich parameters for MC adsorption on the studied materials.

			Langmuir			Freundlich					
			SiO_2			SiO_2			Fe–SiO_2		
pH	T(°C)	I (M)	$K_L \times 10^3$(Lμmol^{-1})	q_{mon} (μmolg^{-1})	r^2	K_F	n	r^2	K_F	n	r^2
4.4	25	0.00	0.85	500.0	0.998	1.38	1.32	0.999	32.86	2.96	0.995
7.0	25	0.00	0.77	357.1	0.999	0.38	1.10	0.999	4.20	1.63	0.999
9.5	25	0.00	0.68	312.5	1.000	0.27	1.08	0.999	0.52	1.15	1.000
4.4	5	0.00	0.78	495.0	0.995	0.73	1.20	0.999	26.45	2.97	0.982
4.4	45	0.00	0.80	498.0	0.995	0.72	1.20	0.997	54.36	2.83	0.992
4.4	25	0.01	0.68	473.9	0.999	0.41	1.14	1.000	21.73	2.79	0.985
4.4	25	0.10	0.67	434.8	0.997	0.36	1.13	1.000	19.51	2.65	0.990
4.4	25	0.30	0.66	416.7	0.995	0.34	1.12	0.999	19.36	2.68	0.989

4. Conclusions

The results shown in this article reveal that the adsorption of MC on the studied solids, from kinetic/isotherms studies, is strongly dependent on pH, increasing as pH decreases. The adsorption capacity at constant pH increases in the order SiO_2 < Fe-SiO_2 mainly due to the presence of Fe_2O_3 particles on the silica support or inside the mesopores offering more active sites for adsorption than silica particles.

The incorporation of a low concentration of iron (1.03 wt.%) on the SiO_2 matrix seems to change the adsorption mechanism. The adsorption of MC on SiO_2 is believed to be related to electrostatic attractions and H-bond formations between amide, carbonylic and phenolic groups of the antibiotic and silica active sites. On the contrary, formation of inner-sphere complexes between the functional groups of the antibiotic and Fe_2O_3 are believed to play a key role in the MC–Fe-SiO_2 system, as deduced from adsorption experiments performed at different KCl concentrations and temperatures. The analysis of thermodynamic parameters suggests that the adsorption on SiO_2 is endothermic and spontaneous in nature although this behavior is not possible to predict for the case of Fe-SiO_2 at all studied temperatures.

The obtained results have a significant importance in environmental and engineering processes, where the production of synthetic materials can play a key role. Mesoporous silica is known to be a very good adsorbent for several species (dyes, pesticides, drugs, heavy metals, etc.) due to the high surface area and pore size. However, since SiO_2 could be modified by the incorporation of metal ions or metal oxides on the mesopore structure, the M-SiO_2 and/or MO_x–SiO_2 (M = metal) systems may act not only as excellent adsorbents but also as alternative photocatalysts for pollution control. This will not only benefit the deactivation of the mentioned pollutants but also reduce their leaching and transport through groundwaters.

Supplementary data to this article can be found online at http://dx.doi.org/10.1016/j.powtec.2013.11.008.

Acknowledgements

This work was financed by SECyT-UNS, CONICET and ANPCYT. MB and MA are members of CONICET. The authors thank Olga Pieroni (Departamento de Química, UNS) for the FT-IR spectra.

References

[1] D. Blum, A. Chtarto, L. Tenenbaum, J. Brotchi, M. Levivier, Clinical potential of minocycline for neurodegenerative disorders, Neurobiol. Dis. 17 (2004) 359–366.
[2] J.P. Bound, N. Voulvoulis, Pharmaceuticals in the aquatic environment—a comparison of risk assessment strategies, Chemosphere 56 (2004) 1143–1155.
[3] A. Pena, M. Paulo, L.J.G. Silva, M. Seifrtová, C.M. Lino, P. Solich, Tetracycline antibiotics in hospital and municipal wastewaters: a pilot study in Portugal, Anal. Bioanal. Chem. 396 (2010) 2929–2936.
[4] C.G. Daughton, T.A. Ternes, Pharmaceuticals and personal care products in the environment: agents of subtle change? Environ. Health Perspect. 107 (1999) 907–938.
[5] Y. Zhao, X. Gu, S. Gao, J. Geng, X. Wang, Adsorption of tetracycline (TC) onto montmorillonite: cations and humic acid effects, Geoderma 183–184 (2012) 12–18.
[6] A.L.P.F. Caroni, C.R.M. de Lima, M.R. Pereira, J.L.C. Fonseca, Tetracycline adsorption on chitosan: a mechanistic description based on mass uptake and zeta potential measurements, Colloids Surf. B 100 (2012) 222–228.
[7] C.T. Kresge, M.E. Leonowicz, W.J. Roth, J.C. Vartuli, J.S. Breck, Ordered mesoporous molecular sieves synthesized by a liquid-crystal template mechanism, Nature 359 (1992) 710–712.
[8] V. Meynen, P. Cool, E.F. Vansant, Verified syntheses of mesoporous materials, Microporous Mesoporous Mater. 125 (2009) 170–223.
[9] Z.A. AlOthman, A.W. Apblett, Synthesis and characterization of a hexagonal mesoporous silica with enhanced, thermal and hydrothermal stabilities, Appl. Surf. Sci. 256 (2010) 3573–3580.
[10] M. Mesa, L. Sierra, J. Patarin, J.L. Guth, Morphology and porosity characteristics control of SBA-16 mesoporous silica. Effect of the triblock surfactant Pluronic F127 degradation during the synthesis, Solid State Sci. 8 (2005) 990–997.
[11] J.Y. Ying, C.P. Mehnert, M.S. Wong, Synthesis and applications of supramolecular-templated mesoporous materials, Angew. Chem. Int. Ed. 38 (1999) 56–77.
[12] M. Brigante, P. Schulz, Synthesis of mesoporous silicas in alkaline and acidic media using the systems cetyltrimethylammonium tosylate (CTAT)–Pluronic F127 triblock copolymer and CTAT–Pluronic F68 triblock copolymer as templates, J. Colloid Interface Sci. 369 (2012) 71–81.
[13] I. Turku, T. Sainio, E. Paatero, Thermodynamics of tetracycline adsorption on silica, Environ. Chem. Lett. 5 (2007) 225–228.
[14] M. Brigante, P. Schulz, Remotion of the antibiotic tetracycline by titania and titania–Silica composed materials, J. Hazard. Mater. 192 (2011) 1597–1608.
[15] M. Brigante, P. Schulz, Adsorption of paraquat on mesoporous silica modified with titania: effects of pH, ionic strength and temperature, J. Colloid Interface Sci. 363 (2011) 355–361.
[16] C.V. Waiman, M.J. Avena, A.E. Regazzoni, G.P. Zanini, A real time in situ ATR–FTIR spectroscopic study of glyphosate desorption from goethite as induced by phosphate adsorption: effect of surface coverage, J. Colloid Interface Sci. 94 (2013) 485–489.
[17] J.C. Zuo, S.R. Tong, X.L. Yu, L.Y. Wu, C.Y. Cao, M.F. Ge, W.G. Song, Fe^{3+} and amino functioned mesoporous silica: preparation, structural analysis and arsenic adsorption, J. Hazard. Mater. 235–236 (2012) 336–342.
[18] T. Mahmood, S.U. Din, A. Naeem, S. Mustafa, M. Waseem, M. Hamayun, Adsorption of arsenate from aqueous solution on binary mixed oxide of iron and silicon, Chem. Eng. J. 192 (2012) 90–98.
[19] Q. Yuan, N. Li, W. Geng, Y. Chi, J. Tu, X. Li, C. Shao, Humidity sensing properties of mesoporousironoxide/silica composite prepared via hydrothermal process, Sensors Actuators B 160 (2011) 334–340.
[20] D. Barreca, W.J. Blau, G.M. Croke, F.A. Deeney, F.C. Dillon, J.D. Holmes, C. Kufazvinei, M.A. Morris, T.R. Spalding, E. Tondello, Iron oxide nanoparticle impregnated mesoporoussilicas as platforms for the growth of carbon nanotubes, Microporous Mesoporous Mater. 103 (2007) 142–149.
[21] P. Fejes, V. Kis, K. Lázár, I. Marsi, J.B. Nagy, Various nano-size iron oxide polymorphs on mesoporous supports I: new mesoporous catalyst supports synthesized in acidic and alkaline media, Microporous Mesoporous Mater. 112 (2008) 377–391.
[22] M.E. Parolo, M.J. Avena, G. Pettinari, I. Zajonkovsky, J.M. Valles, M.T. Baschini, Antimicrobial properties of tetracycline and minocycline–montmorillonites, J. Hazard. Mater. 192 (2011) 1597–1608.
[23] A.I. Vogel, Textbook of quantitative inorganic analysis, 5th ed. Longmans Scientifical & Technical, London, UK, 1960.
[24] R.M. Twyman, Wet Digestion, in: P. Worsfold, A. Townshend, C. Poole (Eds.), 2nd edition, Encyclopedia of analytical science, Vol. 8, Elsevier Science, London, UK, 2005, pp. 146–153.
[25] M. Brigante, P. Schulz, Adsorption of the antibiotic minocycline on cerium(IV) oxide: effect of pH, ionic strength and temperature, Microporous Mesoporous Mater. 156 (2012) 138–144.
[26] Y.S. Ho, G. Mc Kay, Sorption of dyes and copper ions onto biosorbents, Process Biochem. 38 (2003) 1047–1061.
[27] C.E. Zubieta, P.V. Messina, C. Luengo, M. Dennehy, O. Pieroni, P.C. Schulz, Reactive dyes remotion by porous TiO_2-chitosan materials, J. Hazard. Mater. 152 (2008) 765–777.
[28] L. Ji, F. Liu, Z. Xu, S. Zheng, D. Zhu, Adsorption of pharmaceutical antibiotics on template-synthesized ordered micro- and mesoporous carbons, Environ. Sci. Technol. 44 (2010) 3116–3122.
[29] Z. Li, L. Schulz, C. Ackley, N. Fenske, Adsorption of tetracycline on kaolinite with pH-dependent surface charges, J. Colloid Interface Sci. 351 (2010) 254–260.

[30] Y. Wang, J. Ren, X. Liu, Y. Wang, Y. Guo, Y. Guo, G. Lu, Facile synthesis of ordered magnetic mesoporous γ-Fe_2O_3/SiO_2 nanocomposites with diverse mesostructures, J. Colloid Interface Sci. 326 (2008) 158–165.
[31] G. Gu, P.P. Ong, C. Chu, Thermal stability of mesoporous silica molecular sieve, J. Phys. Chem. Solids 60 (1999) 943–947.
[32] K.M.S. Khalil, H.A. Mahmoud, T.T. Ali, Direct formation of thermally stabilized amorphous mesoporous Fe_2O_3/SiO_2 nanocomposites by hydrolysis of aqueous iron (III) nitrate in sols of spherical silica particles, Langmuir 24 (2008) 1037–1043.
[33] G. Ennas, A. Musinu, G. Piccalunga, D. Zedda, D. Gatteschi, C. Sangregorio, J.L. Stanger, G. Concas, G. Spano, Characterization of iron oxide nanoparticles in an Fe_2O_3–SiO_2 composite prepared by a sol–gel method, Chem. Mater. 10 (1998) 495–502.
[34] A. Gervasini, C. Messi, P. Carniti, A. Ponti, N. Ravasio, F. Zaccheria, Insight into the properties of Fe oxide present in high concentrations on mesoporous silica, J. Catal. 262 (269) 224–234.
[35] D.Y. Zhao, Q.S. Huo, J.L. Feng, B.F. Chmelka, G.D. Stucky, Nonionic triblock and star diblock copolymer and oligomeric surfactant syntheses of highly ordered, hydrothermally stable, mesoporous silica structures, J. Am. Chem. Soc. 120 (1998) 6024–6036.
[36] P.I. Ravikovitch, A.V. Neimark, Experimental confirmation of different mechanisms of evaporation from ink-bottle type pores: equilibrium, pore blocking, and cavitation, Langmuir 18 (2002) 9830–9837.
[37] K.S.W. Sing, D.H. Everett, R.A.W. Haul, L. Moscou, R.A. Pierotti, J. Rouquérol, T. Siemieniewska, Reporting physisorption data for gas/solid systems with special reference to the determination of surface area and porosity, Pure Appl. Chem. 57 (1985) 603–619.
[38] K. Gude, V.M. Gun'ko, J.P. Blitz, Adsorption and photocatalytic decomposition of methylene blue on surface modified silica and silica–titania, Colloids Surf. A 325 (2008) 17–20.
[39] Y.M. Liu, J. Xu, L. He, Y. Cao, H.Y. He, D.Y. Zhao, J.H. Zhuang, K.N. Fan, Facile synthesis of Fe-loaded mesoporous silica by a combined detemplation-incorporation process through Fenton's chemistry, J. Phys. Chem. 112 (2008) 16575–16583.
[40] M. Kosmulski, pH-dependent surface charging and points of zero charge: v. update, J. Colloid Interface Sci. 353 (2011) 1–15.
[41] C. Rufier, M. Reufer, H. Dietsch, P. Schurtenberger, Single step hybrid coating process to enhance the electrosteric stabilization of inorganic particles, Langmuir 27 (2011) 6622–6627.
[42] Y. Xu, L. Axe, Synthesis and characterization of iron oxide-coated silica and its effect on metal adsorption, J. Colloid Interface Sci. 282 (2005) 11–19.
[43] T.X. Bui, V.H. Pham, S.T. Le, H. Choi, Adsorption of pharmaceuticals onto trimethylsilylated mesoporous SBA-15, J. Hazard. Mater. 254–255 (2013) 345–353.
[44] Y. Brechbühl, I. Christl, E.J. Elzinga, R. Kretzschmar, Competitive sorption of carbonate and arsenic to hematite: combined ATR–FTIR and batch experiments, J. Colloid Interface Sci. 377 (2012) 313–321.
[45] R. Rahnemaie, T. Hiemstra, W.H. van Riemsdijk, Carbonate adsorption on goethite in competition with phosphate, J. Colloid Interface Sci. 315 (2007) 415–425.
[46] H. Chen, H. Luo, Y. Lan, T. Dong, B. Hu, Yiping Wang, Removal of tetracycline from aqueous solutions using polyvinylpyrrolidone (PVP-K30) modified nanoscale zero valent iron, J. Hazard. Mater. 192 (2011) 44–53.
[47] H. Liu, Y. Yang, J. Kang, M. Fan, J. Qu, Removal of tetracycline from water by Fe–Mn binary oxide, J. Environ. Sci. 24 (2012) 242–247.
[48] L.S. Sillén, Stability constant of metal-ion complexes. Part I — inorganic ligands, The Chemical Society, London, UK, 1971.
[49] G. Lagaly, M. Ogawa, I. Dékány, Clay mineral organic interactions, in: F. Bergaya, B.K. Theng, G. Lagaly (Eds.), Handbook of Clay Sciences, first edition, Elsevier, Oxford, 2006, pp. 309–377.
[50] E.J. Elzinga, D.L. Sparks, Phosphate adsorption onto hematite: an in situ ATR–FTIR investigation of the effects of pH and loading level on the mode of phosphate surface complexation, J. Colloid Interface Sci. 308 (2007) 53–70.
[51] M. D'Arcy, D. Weiss, M. Bluck, R. Vilar, Adsorption kinetics, capacity and mechanism of arsenate and phosphate on a bifunctional TiO_2–Fe_2O_3 bi-composite, J. Colloid Interface Sci. 364 (2011) 205–212.
[52] C. Gu, K.G. Karthikeyan, Interaction of tetracycline with aluminium and iron hydrous oxides, Environ. Sci. Technol. 39 (2005) 2660–2667.
[53] E. Tanis, K. Hanna, E. Emmanuel, Experimental and modeling studies of sorption of tetracycline onto iron oxides-coated quartz, Colloids Surf. A 327 (2008) 57–63.
[54] F. Chen, C. Zhou, G. Li, F. Peng, Thermodynamics and kinetics of glyphosate adsorption on resin D301, Arab. J. Chem. (2013), http://dx.doi.org/10.1016/j.arabjc.2012.04.014(in press).
[55] D.P. Rodda, B.B. Johnson, J.D. Wells, Modeling the effect of temperature on adsorption of lead(II) and zinc(II) onto goethite at constant pH, J. Colloid Interface Sci. 184 (1996) 365–377.
[56] G. Sposito, The surface chemistry of natural particles, Oxford University Press, New York, USA, 2004.
[57] W.A. House, Adsorption in heterogeneous surfaces, in: D.H. Everett (Ed.), Colloid Science, Vol. 4, RSC Publishing, Canbridge, UK, 1983, pp. 1–58.
[58] M. Liu, L. Hou, S. Yu, B. Xi, Y. Zhao, X. Xia, MCM-41 impregnated with A zeolite precursor: synthesis, characterization and tetracycline antibiotics removal from aqueous solution, Chem. Eng. J. 223 (2013) 678–687.
[59] Y. Zhao, J. Geng, X. Wang, X. Gu, S. Gao, Adsorption of tetracycline onto goethite in the presence of metal cations and humic substances, J. Colloid Interface Sci. 361 (2011) 247–251.

Maximiliano Brigante, PhD, is an Assistant Researcher of the Consejo Nacional de Investigaciones Científicas y Técnicas de la República Argentina (CONICET). His field of research involves environmental chemistry, water remediation and solid-state synthesis and he has more than 10 articles published on these fields in the last 3 years. M. Brigante is Associate Professor at the Universidad Nacional del Sur (Argentina).

Maria Eugenia Parolo, PhD, is a Teaching Assistant at the Universidad Nacional del Comahue (Argentina). Her research interest is focused on solid–water interface, especially in the possible use of clays and several soil components in pharmaceutical applications.

Pablo Carlos Schulz, PhD, is a senior researcher of the highest level in the scientific system in the Argentinian universities. He is an Extraordinary Consultus Professor at the Universidad Nacional del Sur (Argentina) and Chief of the Research Department at the School of Officers, an academic unit of the Argentine Navy University Institute. His research interest is focused on surfactant science and he has about 150 articles published on this field.

Marcelo Avena, PhD, is an Independent Researcher of the CONICET and a Professor at the Universidad Nacional del Sur (Argentina). His field of research involves inorganic and physical chemistry of the solid–liquid interface; synthesis, dissolution and aging of metal oxides; chemical minerals, clays and silts; physical chemistry of humic substances; and environmental inorganic chemistry, which includes a) Control and preservation of water resources: water quality and eutrophication and b) Speciation of contaminants in the environment. M. Avena published about 60 articles in medium and high-impact journals.